ACS Catalysis

Research Article

pubs.acs.org/acscatalysis

Dehydration of Glycerol to Acrolein over Hierarchical ZSM-5 Zeolites: Effects of Mesoporosity and Acidity

Hongbin Zhang,[†] Zhijie Hu,[†] Liang Huang,[†] Hongxia Zhang,[†] Kunshan Song,[†] Lei Wang,[†] Zhangping Shi,[†] Jianxue Ma,[‡] Yan Zhuang,[‡] Wei Shen,[†] Yahong Zhang,[†] Hualong Xu,*[,†] and Yi Tang*[,†]

[†]Department of Chemistry, Laboratory of Advanced Materials, Shanghai Key Laboratory of Molecular Catalysis and Innovative Materials and Collaborative Innovation Center of Chemistry for Energy Materials, Fudan University, Shanghai 200433, China

[‡]Shanghai Huayi Acrytic Acid Co., Ltd., Shanghai 200137, China

Supporting Information

ABSTRACT: Selective dehydration of glycerol to value-added acrolein is an interesting catalytic process not only owing to the increasing coproduction of glycerol in the biodiesel production but also due to the emerging perspectives to provide a sustainable route for acrolein production. The use of zeolites in glycerol dehydration is a very promising way with high performance, but these microporous catalysts are often severely constrained by the rapid catalyst deactivation due to coke formation. Although the introduction of hierarchical structure in microporous zeolite crystals is believed to be an effective approach to enhance their activity and lifetime, the relationship between the mesoporosity and catalytic performance is still controversial. In this paper, four kinds of typical hierarchical ZSM-5 catalysts with diverse mesoporosity and similar microporosity/acidity are prepared by the salt-aided seed-induced route. By systematically studying their catalytic performances, the effects of various mesopore types on the glycerol dehydration are declared, including pore size, amount, distribution, and connectivity. The sample with open and interconnected mesopore architecture display the high activity, long lifetime, and improved selectivity, while the worse behavior of closed and small mesopores is attributed to the mass transfer limitations and/or the in-pore condensation of reactant or its heavier derivatives. Moreover, the combined effect of acidity and hierarchical structure was also explored by changing the framework Si/Al ratio. The findings emphasize the necessity of reasonably designing the zeolite catalysts with proper hierarchical structure and acidity for maximal catalytic advantage.

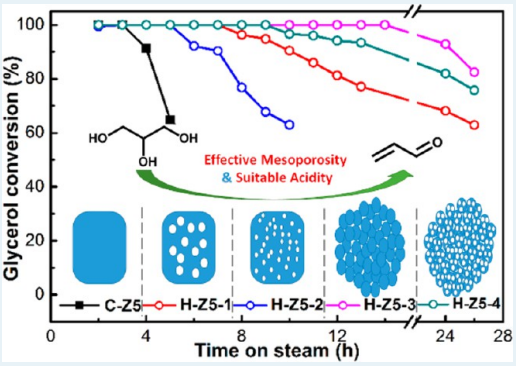

KEYWORDS: *zeolite, hierarchical structure, acidity, glycerol dehydration, structure-performance relationship*

1. INTRODUCTION

Biomass conversion has attracted much attention for its possibility to replace, stepwise, traditional petroleum-based chemical processes.[1−3] Among these emerging biomass-based processes, glycerol conversion is considered to be an important and promising approach for its rapidly increasing coproduction in the biodiesel production process and its capability to synthesize various chemicals as a platform molecule.[4−8] Dehydration of glycerol is one of the most interesting catalytic processes because of its perspective to provide a sustainable route for acrolein production for industrial and agricultural applications.[4−7] Consequently, for the purpose of developing a high-performance heterogeneous catalyst for the glycerol dehydration to acrolein, various solid acid catalysts have been applied to this process in either gaseous or liquid phases, including heteropoly acids and other supported inorganic acids,[9−11] mixed-oxides,[12−14] acidic zeolites,[15−22] and so on.

Zeolites have been widely used in a number of petrochemical processes and biomass conversions because of their well-defined micropore structures, large surface areas, strong acidity, and high hydrothermal stability.[23,24] Recently, acidic zeolite catalysts, especially ZSM-5 zeolite with special 10-membered ring intersecting channel system, have been confirmed to be a good alternative in the gaseous phase dehydration of glycerol to acrolein.[15−17,20−22,25,26] The high-crystalline microporous framework and Brønsted acid nature endow them with high activity and outstanding selectivity of acrolein.[16,17] However, the major drawback of zeolites is the rapid deactivation caused by the formation of coke which would cover the active sites or block the microchannels in the catalysts.[5−7,18,19,26−29] The sole microporous structure in traditional zeolite crystals seriously restricts their catalytic applications due to the mass transfer limitations.[30−32] Recently, numerous studies have been reported to synthesize hierarchical structured zeolites, and the provision of the secondary network of meso- and/or macropores plays an important role to improve their catalytic

Received: December 14, 2014
Revised: March 6, 2015
Published: March 11, 2015

DOI: 10.1021/cs5019953
ACS Catal. 2015, 5, 2548−2558

properties in a wide range of important reactions.[30−37] The catalytic performance closely depends on the quality of the mesopores, including their size, distribution, and connectivity, to some extent.[38,39]

However, up to now, it is still unclear and controversial what type of hierarchical porosity is suitable for the glycerol dehydration and how it takes effect. Jia et al.[18] investigated the catalytic performances of nanosized HZSM-5 and bulk HZSM-5 with similar Si/Al ratios and illustrated that the zeolites with short micropores were more suitable for glycerol dehydration. Conversely, Possato et al.[19] performed a systematic study on the gaseous phase dehydration of glycerol using microporous MFI zeolites and alkaline-desilicated mesoporous ones, in which all of the samples showed rather similar catalytic performance although their coke contents increased with the mesoporous volume. The effect of textural properties also has been investigated on heteropoly acids and mixed oxides,[5−7,9,40] and some abnormal observations showed that these catalysts with small-sized mesopores sometimes displayed a relatively low activity or a relatively fast deactivation.[9,11,12,14] According to the Kelvin equation,[41] Hulteberg et al.[27] proposed an explanatory model and claimed that the glycerol pore condensation in mesopores followed by the polymerization reactions may play an important role in catalyst activity and deactivation. Furthermore, with the creation of mesopores within zeolite crystals or the reduction of crystal size to nanoscale, more framework defects may appear in the catalysts, such as extraframework aluminum, hydroxyl nests (or siloxy sites), and terminal silanol groups.[33,35,36,42] These would generally lead to a lower hydrothermal stability and an increasing formation of undesired byproducts related to Lewis acid sites.[5−7,16,18,29] Therefore, on the basis of results mentioned above, it is still a great challenge to find a suitable zeolite catalyst with proper hierarchical structure and acidic property for the dehydration of glycerol to acrolein.

More recently, by adopting the environmentally friendly, low-cost "salt-aided seed-induced route" developed in our group, hierarchical ZSM-5 zeolites with two typical mesopore topologies, called "enriched intracrystal mesoporous zeolite" and "nano-crystallite oriented self-assembled zeolite", could be facilely fabricated by simply changing the gel compositions and reaction conditions.[33,34] Furthermore, these hierarchical zeolites and their isomorphous substituted analogues have shown remarkable performances in a number of catalytic processes, such as isomerization of *o*-xylene, butene cracking, methanol to propylene, and low-density polypropylene cracking.[33,34,37] In this study, by deliberately adjusting the composition of the gel precursor, the following four typical catalysts with a series of mesopore architectures are successfully constructed, covering the properties of mesopore size, amount, distribution, and connectivity:

- Sample H-Z5-1 possesses large size but a lesser amount of closed intracrystal mesopores.
- Sample H-Z5-2 has small size but more closed intracrystal mesopores.
- Sample H-Z5-3 possesses abundant open intercrystallite mesopores due to its nanocrystallite oriented self-assembled structure.
- Sample H-Z5-4 combines the structures of intra- and intercrystal mesopores with special self-assembled structures of nanocrystallite containing intracrystal mesopores.

In order to reasonably analyze the role of different mesopore architectures on catalytic behaviors of glycerol dehydration, the catalytic performances of different catalysts were investigated under the same reaction conditions, and the catalyst's intrinsic microporsity and acidity were regulated to a similar level. Besides, the influence of the acidity in zeolite catalysts was also explored by changing the Si/Al ratio on two typical hierarchical structured catalysts. The effects of mesopore topologies as well as acidity of hierarchical zeolites discussed here will be greatly practical and significant for designing the catalysts with most adequate porous and acidic properties for biomass conversions with high activity, selectivity, and stability.

2. EXPERIMENTAL SECTION

2.1. Catalyst Preparation. The four typical hierarchical structured ZSM-5 catalysts were synthesized according to our previously reported "salt-aided seed-induced route"[33,34,37] in a starting aluminosilicate gel with the components of $1SiO_2$:0.004 Al_2O_3:0.15 Na_2O:0.1 TPABr:0.3 KF:xH_2O. By this method, the samples of H-Z5-1, H-Z5-2, H-Z5-3, and H-Z5-4 with different mesopore topologies can be facilely obtained by changing the water content as x = 30, 45, 75, and 60, respectively. The typical process for the sample preparation is briefly described as below, and the detailed evolution of the mesopore structure and its relationship with the preparation conditions will be reported in the near future. After mixing the colloidal silica with the preset solutions of NaOH, $Al_2(SO_4)_3{\cdot}18H_2O$, KF, and TPABr under vigorous stirring, the colloidal solution of preprepared silicalite-1 seed with the crystal size of 200 nm was added into the gel. The addition quantity of seed solution typically equaled to 7.0 wt % of total SiO_2 weight in the starting gel. The silicalite-1 seeds were synthesized by a clear solution method and the obtained silicalite-1 suspension was directly used as seed without further treatment. After aging under stirring at ambient temperature for 2−8 h, the mixture was hydrothermally treated at 120 °C for 24 h. The zeolite products were recovered by filtration, washed with deionized water, dried at 90 °C for 12 h, and finally calcined under static air at 550 °C for 5 h. The final acidic zeolite catalysts of H-Z5-x were obtained by ion-exchange with NH_4NO_3 solution for three times at 90 °C for 3 h and calcination at 550 °C for 5 h. The residue Na^+ or K^+ ion contents in them were all lower than the detection limit of X-ray fluorescence (XRF) characterization.

To detect the effect of acidity on the catalytic performance for the glycerol dehydration, two typical hierarchical ZSM-5 catalyst analogues to H-Z5-1 and H-Z5-3 but with lower Si/Al ratio were employed to the glycerol dehydration, which were prepared by exactly the same methods as reported in our recent work.[33,34,37] They were renamed as H-Z5-1-L with large enriched intracrystal mesopores[34] and H-Z5-3-L with nanocrystallite oriented self-assembled structure,[33] respectively.

Additionally, two conventional H-ZSM-5 samples with high Si/Al (denoted as C-Z5) and low Si/Al ratios (C-Z5-L) were also employed as references to investigate the advantages of hierarchically structured ZSM-5 catalysts. These two conventional samples were purchased from Nankai Catalyst Company, Tianjin, China.

2.2. Catalyst Characterization. The morphology, mesopore structure, and related element mapping information were obtained by field emission scanning electron microscope (FESEM, Hitachi S-4800) and transmission electron microscope (TEM, JEOL JEM-2011, and FEI Tecnai G2 F20 S-Twin), respectively. Chemical analyses were performed by XRF

DOI: 10.1021/cs5019953
ACS Catal. 2015, 5, 2548−2558

with a Bruker-AXS spectrometer. The N_2- and Ar-sorption isotherms were measured by a Micromeritics ASAP-2010 instrument at liquid nitrogen temperature and an Autosorb IQ_2 analyzer at liquid argon temperature, respectively. The mercury intrusion porosimetry was performed with a Micromeritics Autopore IV 9500 following in situ sample evacuation to characterize the information for mesopores with open structure. The samples were evacuated at 573 K for 12 h prior to the characterization. The crystalline structures were characterized by X-ray diffraction (XRD) on a Bruker D8-Advanced diffractometer with Cu Kα radiation at 40 kV and 40 mA. The magic angle spinning nuclear nuclear magnetic resonance (MASNMR) experiments were performed on a Bruker DSX 300 spectrometer. The acid amount and strength were determined by NH_3-temperature-programmed desorption (NH_3-TPD) using a Micromeritics AutoChem 2920 analyzer. The catalyst sample (0.1 g) was heated at 550 °C in a He flow for 3 h and then cooled to 80 °C. NH_3 adsorption was performed under a flow of 10 vol % NH_3/He (30 mL/min) for 1 h. The NH_3-TPD was promptly started at a heating rate of 10 °C/min from 80 to 600 °C. Fourier transform infrared (FTIR) spectroscopy measurements were performed by a Nicolet FT-IR 360 spectrometer. The samples were pressed into thin wafers and were degassed in a vacuum cell for 30 min at 400 °C. Then, the sample was cooled down to room temperature, and a background spectrum was recorded. Next, consecutive doses of pyridine were added to the sample until saturation. Finally, the sample was heated to 320 °C under vacuum environment for 2 h, and the spectra were then recorded. The amount of accessible acid sites of zeolites was determined by a nonaqueous titration on a potentiometric titration meter (ZDJ-5, Shanghai Leici Instrument Factory) using *tert*-butylamine. The catalyst was dried in flowing air at 723 K for 2 h and then dispersed in acetonitrile. After being agitated for 3 h, the suspension was titrated by *tert*-butylamine solution in acetonitrile at a rate of 0.1 mL/min. The electrode potential variation was measured with a double junction electrode. The measurement of o-xylene diffusion in ZSM-5 zeolites was performed using a computer-controlled intelligent gravimetric analyzer (IGA, Hiden Analytical Ltd., Warrington, UK). The sample was degassed under a vacuum of less than 10^{-3} Pa at 673 K for 2 h prior to the adsorption measurement.

2.3. Catalytic Performance Measurement. The gaseous phase dehydration of glycerol over all catalysts was conducted under atmospheric pressure in an automatic fixed-bed micro-reactor (inner diameter, I.D. = 8 mm). An aqueous glycerol solution with glycerol/H_2O weight ratio of 1:4 was used as the feed. The reaction temperatures were selected at 250, 280, 300, and 320 °C, and weight hourly space velocity (WHSV) values were 2.4 or 12 h^{-1} according to the aims of experiments. The pressed catalyst (20−40 mesh) was placed in the central region of the reactor, with each end filled with quartz sand. Before the reaction, the catalyst was activated with N_2 for 2 h.The reaction products were condensed in a cold trap and collected hourly for analysis on a gas chromatographs equipped with a flame ionization detector (FID) and a TR-Wax capillary column (I.D. = 0.25 mm and length = 30 m). The conversion of glycerol and the product selectivity were calculated according to the adopted method and the relative mass correction factors of the product compounds shown in ref 18. The coke amounts of the catalysts in the initial reaction period of 2−3 h and after deactivation were measured on a thermal gravimetric analyzer (TGA, NETSCH, STA 449-F3) in an air flow.

3. RESULTS AND DISCUSSION

3.1. Characterization on Hierarchical Porous Structure. In order to assess the impact of mesopore architecture on the glycerol dehydration reaction, the priority is to prepare samples with a series of defined specific hierarchical porous structures. Four typical hierarchical ZSM-5 catalysts of H-Z5-1, H-Z5-2, H-Z5-3, and H-Z5-4 are obtained through our previously developed salt-aided seed-induced route.[33,34,37] FE-SEM and TEM were first employed to characterize their morphologies and mesopore structures. According to the FE-SEM images in Figure 1, these hierarchically structured samples

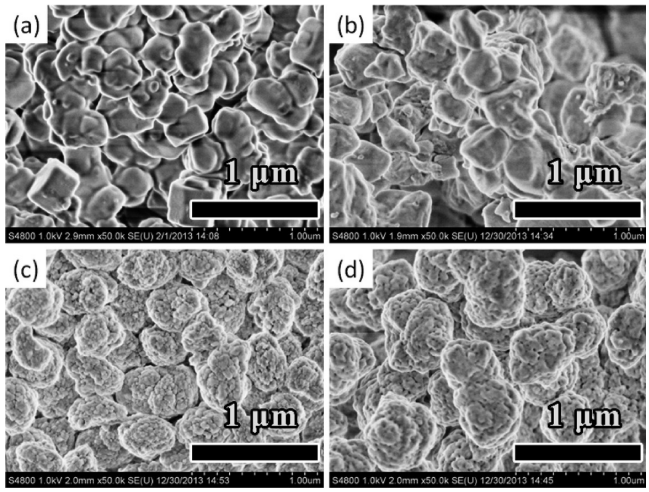

Figure 1. SEM images of (a) H-Z5-1, (b) H-Z5-2, (c) H-Z5-3, and (d) H-Z5-4.

can be divided into two categories. H-Z5-1 and H-Z5-2 exhibit the irregular morphologies with relatively smooth external surface, while H-Z5-3 and H-Z5-4 display the uniform globular and sponge-like morphologies with rough external surface. All the samples possess almost the same particle size of 400−600 nm. Figure 2 displays the representative TEM images of these four HZSM-5 samples which can reveal the differences of the hierarchical porous structures more clearly. Obviously, the H-Z5-1 (Figure 2a and b) and H-Z5-2 (Figure 2c and d) with irregular-shaped single-crystal particles are pervaded with enriched randomly oriented mesopores embedded in their micropore framework. Such mesopore architecture is very similar to the sample of "enriched intracrystal mesoporous structure" reported in our previous paper.[34] Moreover, it is worthy to notice that the size and amount of the mesopores in these two samples are somewhat different: H-Z5-1 possesses relatively large size (about 20−80 nm) but less mesopores, while H-Z5-2 has the smaller size (about 5−30 nm) but more mesopores. For H-Z5-3 in Figure 2e and f, these crystals display the morphologies of uniform zeolite microspheres which are made up of abundant individual small nanocrystallite domains with an average diameter of about 20−40 nm, which is similar to the earlier reported "nano-crystallite oriented self-assembled structure".[33,37] This in situ self-assembled structure with abundant small nanocrystallites will give rise to abundant open intercrystallite mesopores. Very interestingly, as shown in Figure 2g and h, the H-Z5-4 sample shows the special nanocrystallite self-assembled structure but with intracrystal mesopores in most of the small composited nanocrystallites. This structure can be considered as the combination of

DOI: 10.1021/cs5019953
ACS Catal. 2015, 5, 2548−2558

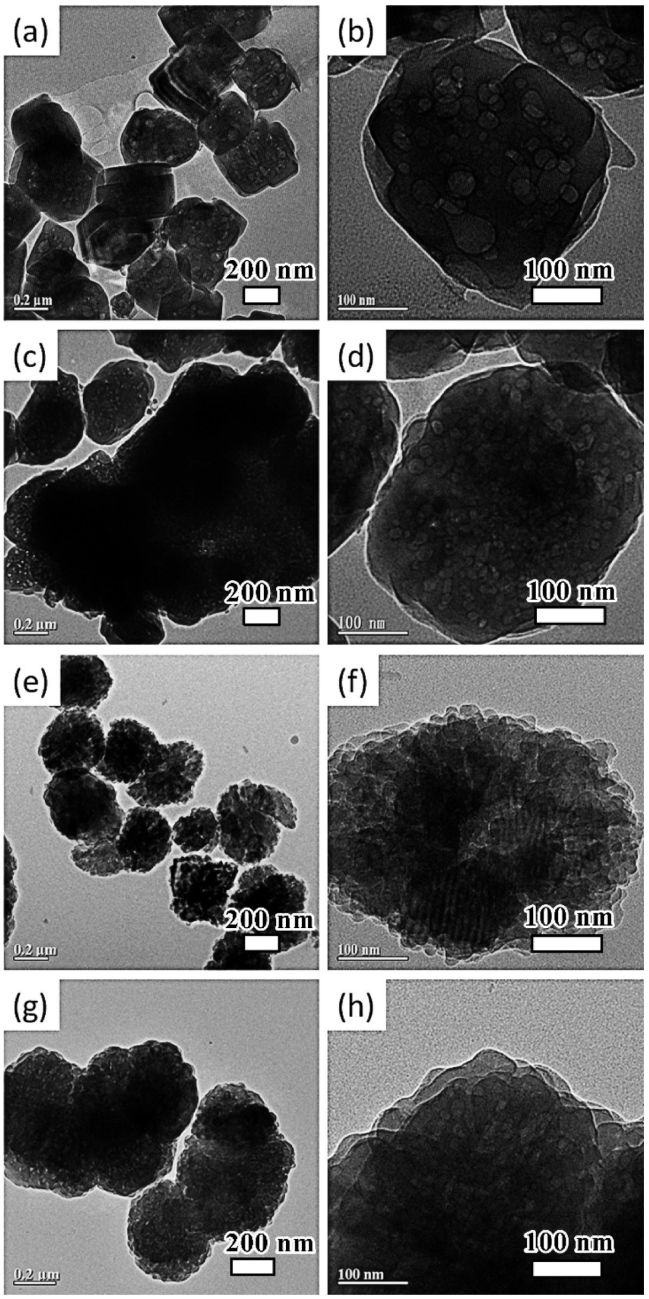

Figure 2. TEM images of (a–b) H-Z5-1, (c–d) H-Z5-2, (e–f) H-Z5-3, and (g–h) H-Z5-4.

nanocrystallite assembled structure of H-Z5-3 and intracrystal mesoporous architecture of H-Z5-2. These specific hierarchical structures may interconnect the micropores more effectively to offer additional diffusional paths for guest molecules.

The differences in these hierarchical porous structures are also evidenced by the N_2 sorption results (Figure 3a), in which the four samples all show a type IV isotherm but with different shaped hysteresis loops, indicating their subtle distinctions in hierarchical porous structure.[33,34,43,44] The steep increases of these four sample at very low relative pressure (P/P_0 < 0.1) illustrate their perfect microporosity, while the hysteresis loops appearing at P/P_0 = 0.1–0.3 are associated with the phenomenon of fluid-to-crystalline phase transition of adsorbed N_2 usually for the ZSM-5 zeolite with a high Si/Al ratio.[43] At high relative pressures (P/P_0 = 0.4–1.0), both of H-Z5-1 and

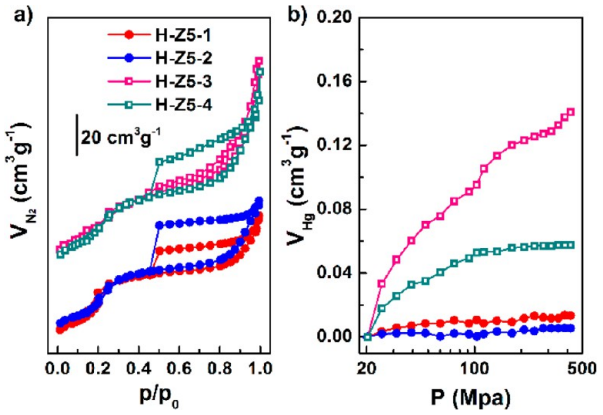

Figure 3. (a) N_2 sorption isotherms at 77 K and (b) Hg intrusion curves from 20 to 418 MPa of different hierarchical zeolite catalysts. For the sake of clarity, the isotherms of H-Z5-3 and H-Z5-4 are shifted 30 cm^3/g upward.

H-Z5-2 possess the additional type-H4 hysteresis loops with a characteristic step down on the desorption branch around P/P_0 = 0.43. These special hysteresis loops are ascribed to the tensile strength or cavitation effect of ink-bottle type mesopores, in which the desorption of the adsorbent from the pore body suddenly occurs after emptying its neck (either micropores or entrances <4 nm).[34,43,44] This result is consistent with the observation in TEM images (Figure 2a–d) and reflects most mesopores are occluded or constricted in the H-Z5-1 and H-Z5-2 crystals. It can be also observed that the size of the hysteresis loop (namely the adsorption volume difference between desorption and adsorption branches) for H-Z5-2 is larger than that of H-Z5-1, and the enhanced adsorption of H-Z5-2 at intermediate pressures ($0.2 < P/P_0 < 0.9$) is also earlier than that of H-Z5-1. These phenomena indicate that H-Z5-2 has the smaller size but more amount of mesopores, in accordance with TEM results. Different from the samples with enriched intramesopore structure (H-Z5-1 and H-Z5-2), the H-Z5-3 shows a type-H3 hysteresis loop, where a continuously enhanced adsorption appears at intermediate and high pressures ($0.4 < P/P_0 < 1$) without the characteristic step down around P/P_0 = 0.43 in the desorption branch. This H3 hysteresis loop arises from nitrogen adsorption on the open intercrystallite mesopores formed by the assembly of adjacent nanocrystallites,[33] in agreement with the TEM images in Figure 2e and f. Moreover, H-Z5-4 displays a special hysteresis loop combining the type-H3 and H4, which further supports its special structure of self-assembled nanocrystallite with intracrystallite mesopores (see Figure 2g and h). The textural properties of all samples are summarized in Table 1 which are calculated according to the isotherms in Figure 3a. All samples have large specific surface area (S_L, ca. 470 m^2/g) and micropore volume (V_{micro}, ca. 0.12 cm^3/g), indicating their high crystallinity. H-Z5-1 and H-Z5-2 possess large mesopore volume (V_{meso}, ca. 0.16 cm^3/g) but small mesopore surface area (S_{meso}, ca. 65 m^2/g); while H-Z5-3 and H-Z5-4 possess large mesopore volume (V_{meso}, ca. 0.20 cm^3/g) and large mesopore surface area (S_{meso}, ca. 110 m^2/g). These results well verify their different mesopore architectures.

An argon adsorption measurement at 87 K has further been applied to properly assess the micro- and mesopores in these four materials. The high-resolution isotherms (Figure S1a) at low relative pressure indicate their analogous adsorption

DOI: 10.1021/cs5019953
ACS Catal. 2015, 5, 2548–2558

Table 1. Textural Properties and Chemical Composition of Different Zeolite Catalysts

sample	Si/Al[a]	S_L m^2/g	S_{meso}[b] m^2/g	V_{micro}[b] cm^3/g	$V_{meso,N2}$[c] cm^3/g	$V_{meso,Hg}$[d] cm^3/g
C-Z5	99	458	49	0.13	0.05	0.00
H-Z5-1	100	472	71	0.12	0.14	0.01
H-Z5-2	105	456	62	0.12	0.17	0.00
H-Z5-3	110	508	115	0.12	0.21	0.14
H-Z5-4	102	460	108	0.11	0.19	0.06

[a]Determined by XRF. [b]By *t*-plot method.[38] [c]Using the BJH method. [d]Derived from Hg intrusion curve (20−418 MPa). S_L: Langmuir surface area. S_{meso}: mesopore surface area.[38] V_{micro}: micropore volume. V_{meso}: mesopore volume.

properties in micropores, suggesting preservation of the zeolitic microporous framework structure, whereas the enhanced uptake of these hierarchical samples at higher relative pressures is in accordance with their unique mesoporosity as indicated by N_2 adsorption. The micropore size distributions (Figure S1b) derived from the argon adsorption isotherms using the nonlocal density functional theory (NLDFT) pore size model evidently confirm that the zeolitic micropore size (around ca. 0.55 nm) is not affected by the introduction of mesopores. The mesopore size distribution (Figure S1c) also shows evidence of their diverse mesoporosity. H-Z5-1 displays a similar curve shape with H-Z5-2, but the curve of H-Z5-2 presents a larger mesopore quantity and seems to center at a slightly small pore diameter. Different from these two samples, H-Z5-3 shows the widest pore size distribution which centers at the range of relative smaller as well as larger diameter, probably rooting in its nanocrystallites assembly structure. The curve of H-Z5-4 looks similar to that of H-Z5-2. Considering the huge differences of mesopore structures among these hierarchical samples as well as the pore mode applied in BJH method, the comprehensive understanding on the mesopore architectures should refer to the results drawn from all other characterizations.

Besides, Hg intrusion experiments are applied to discriminate the relative accessibility of mesopores of different samples, because Hg can only penetrate into the mesopores larger than 4 nm in diameter (the highest pressure is around 418 MPa) from the external surface of crystals.[38,39] As shown in Figure 3b, hardly any mercury can penetrate into the crystals of H-Z5-1 and H-Z5-2 at higher pressures, indicating no significant accessible mesoporosity in these samples. While in the H-Z5-3 crystals, a distinct intrusion occurs in the pressure range of 20−418 MPa, corresponding to the pore size of 4−80 nm. Comparing the value of V_{meso} measured by N_2 sorption and that by Hg intrusion (Table 1), the results reveal that almost 70% of the mesopore volume determined by N_2 sorption is accessible to mercury in H-Z5-3, whereas the fraction of accessible mesopores in H-Z5-4 is only 30%, even nearly zero for H-Z5-1 and H-Z5-2. These findings verify that the mesopores in H-Z5-1 and H-Z5-2 are occluded, the mesopores in H-Z5-3 mostly open to the external surface, while H-Z5-4 falls in between.

The high-angle annular dark-field scanning TEM (HAADF-STEM) is also conducted to gain more evidence on the mesopore quality (Figure 4a). Compared with the results of SEM and TEM (Figures 1 and 2), the HAADF-STEM images not only display the smooth and regular particle edge of H-Z5-1 and H-Z5-2 contrasting with the rough surfaces of H-Z5-3

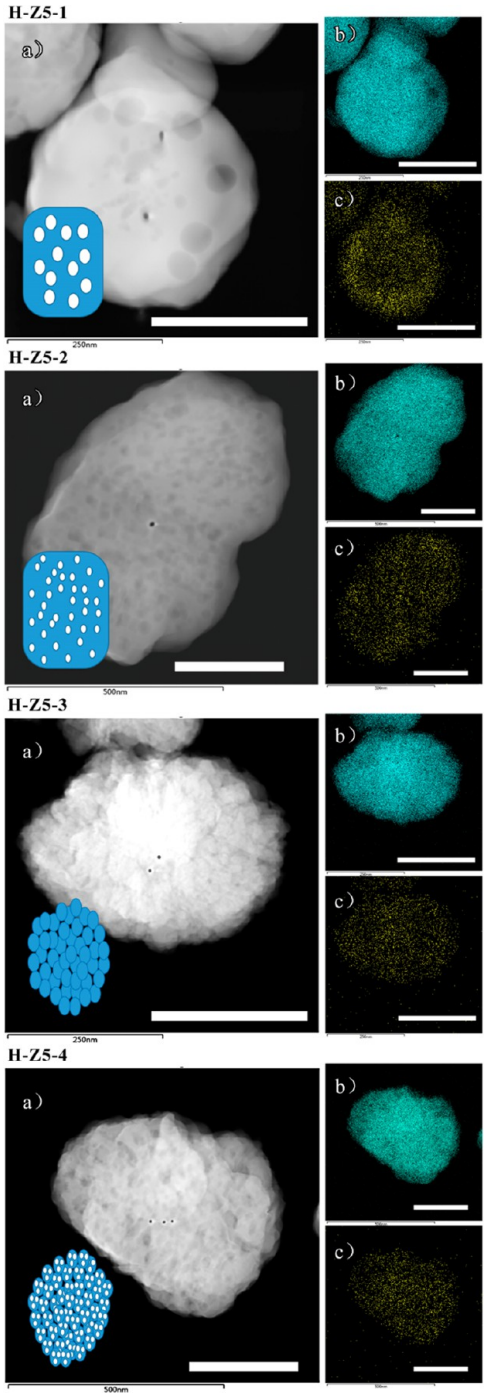

Figure 4. (a) HAADF-STEM images, (b) Si mapping images, and (c) Al mapping images of different hierarchical zeolite materials. All scale bars in micrographs indicate 250 nm. The insets in part a are the schematic illustrations of the pore structures for visualization.

and H-Z5-4 but also show evidence of the presence of diverse mesoporosity in these samples. The H-Z5-1 and H-Z5-2 possess the occluded mesopores but with various amount/size, while H-Z5-3 has enriched open mesopores between nanocrystallite domains, and H-Z5-4 looks like owning both types of mesopores appeared in H-Z5-2 and H-Z5-3. Moreover, the spatial distribution of the elemental composition in the zeolite crystals is detected including detailed point analysis of silicon, aluminum, and oxygen and shown in Figures 4b and c and S2,

DOI: 10.1021/cs5019953
ACS Catal. 2015, 5, 2548−2558

respectively, which confirms the minor local differences in concentration of the various elements.

By summarizing the characterization results on both the hierarchical porous and textural properties shown above (Figures 1−4 and Table 1), the schematic illustration of the pores structure of these four H-Z5-x (x = 1, 2, 3, and 4) samples are depicted in the insets of Figure 4a for visualization: H-Z5-1 and H-Z5-2 belong to the occluded intracrystal mesoporous ZSM-5 zeolite, but the former has a relative larger size and less amount of mesopore. H-Z5-3 is nanocrystallite oriented self-assembled ZSM-5 zeolite which mainly has the open intercrystallite mesopores. H-Z5-4 combines the above two kinds of structures, i.e., the self-assembled structure of nanocrystallite probably with close intramesopores in the crystallites. The particle sizes of these four samples are all about 400−600 nm. These hierarchical porous structures with different pore size, distribution, and connectivity may provide good models to inspect the influence of the mesopore type on their catalytic performances.

3.2. Characterization on Framework and Surface Acid Property. For more clearly studying the effects of hierarchical porous structure in the glycerol dehydration reaction, it is necessary to modulate these hierarchical zeolites with similar bulk characteristics, including intrinsic microposity, the framework crystallinity, and acidity. A conventional ZSM-5 (denoted as C-Z5) is adopted as the reference sample for the comparison and some of its physicochemical properties are also listed in Table 1. C-Z5 sample presents similar specific surface area and microporous volume with other four samples, but its mesoporous volume and external surface are smaller. Figure S3 depicts the XRD patterns of these five ZSM-5 samples. They all present the characteristic diffraction peaks at 2θ of 7.0−9.0 and 23.0−25.0 representing the typical MFI structure, and no impure or amorphous phase is detected. The H-Z5-3 and H-Z5-4 samples present slightly broader and weaker diffraction peaks, probably due to the small-sized intergrowing nanocrystallites in the hierarchical structure.

The content, distribution, and state of aluminum species in framework exert pivotal influence on the acidity of zeolite catalyst. Table 1 shows the similar Si/Al ratios of various samples determined by XRF measurement. Therefore, the aluminum contents or the acid site amounts in these samples are almost the same (supposing one aluminum atom represents one acid site). Moreover, the aluminum distributions of these samples also display minor local concentration differences (Figure 4c). Figure 5 presents the ^{27}Al MAS NMR spectra of these samples. All samples exhibit a main resonance (>97%) located at 56 ppm corresponding to the tetrahedral coordination framework aluminum atoms with Brønsted acid nature. The Brønsted acid sites are expected to be the main active sites for the glycerol dehydration to acrolein.[6,7,18,20,21,28,29] Besides, only a very weak signal exists on C-Z5 at 3 ppm, indicating the existence of few octahedral extra-framework aluminum species with Lewis acid nature. All of these hierarchical zeolites synthesized by the novel "salt-aided seed-induced route" have almost no signal at 3 ppm, further indicating their perfect framework crystallinity without extra-framework aluminum species.

NH_3-TPD is adopted to provide the information on the amount and strength of acid sites. Figure S4 displays the typical two-peak curves for the normal zeolite catalysts, and the corresponding quantitative results are shown in Table 2. The low-temperature peak (peak I) and the high-temperature one

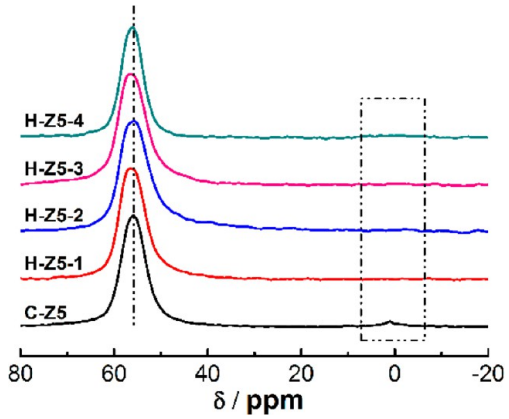

Figure 5. ^{27}Al MAS NMR spectra of different catalysts.

Table 2. Acidities of Different Zeolite Catalysts

	peak temperature in NH_3-TPD (°C)		acid amount in NH_3-TPD (mmol/g)			acid concerntration in pyridine -IR (%)	
sample	peak I	peak II	c_w [a]	c_s [a]	total	c_B [b]	c_L [b]
C-Z5	157.9	353.4	0.059	0.101	0.160	94	6
H-Z5-1	165.9	351.2	0.064	0.102	0.166	93	7
H-Z5-2	168.9	357.5	0.061	0.087	0.148	90	10
H-Z5-3	168.9	354.6	0.056	0.089	0.145	94	6
H-Z5-4	162.4	341.3	0.058	0.097	0.155	94	6

[a]Amount of weak (c_w) and strong (c_s) acid sites at peaks I and II determined by NH_3-TPD. [b]Concentration (%) of Brønsted (c_B) and Lewis (c_L) acid sites determined by pyridine-IR using extinction coefficients of $\varepsilon_{(Brønsted)}$ = 1.67 cm/μmol and $\varepsilon_{(Lewis)}$ = 2.94 cm/μmol.

(peak II) are assigned to the weak and strong acid sites, respectively; and the area under the curve represents the corresponding acid amount. As shown in Figure S4 and Table 2, all of the samples present almost the same desorption peak temperature at about 160 °C for peak I and 350 °C for peak II, and their acid amounts calculated from the ammonia desorption are 0.060 ± 0.004 and 0.095 ± 0.008 mmol/g for peaks I and II, respectively, indicating their similar acid site amount and strength distribution.

The accessibility of acid sites to relative large molecule is also assessed by a nonaqueous potentiometric titration measurement with *tert*-butylamine as the titrant, where the solvent diameter of *tert*-butylamine (ca. 0.68 nm) is larger than the micropore size of ZSM-5 zeolite (ca. 0.54 nm). As shown in Figure S5, the numbers of accessible acid sites are very low for the samples with closed intracrystal mesopores (H-Z5-1 and H-Z5-2); while the numbers elevate largely for the samples with enriched open mesopores (e.g., H-Z5-3 and H-Z5-4), and H-Z5-3 presents the best accessibility of acid sites among all samples. If we define the titration amount of *tert*-butylamine at $E \geq 50$ mV as the knee point to calculate the accessible acid amount, their acid site accessibilities follow the order of H-Z5-3 > H-Z5-4 > H-Z5-1 ≈ H-Z5-2 ≈ C-Z5, which matches well with the trend of Hg intrusion data in Figure 3b. This titration result further confirms our previous observations with respect to the mesopore architectures of these four samples.

The acid type also plays a crucial role on the reaction activity and selectivity. The FT-IR spectra after pyridine adsorption (pyridine-IR) were conducted to distinguish the Brønsted and

DOI: 10.1021/cs5019953
ACS Catal. 2015, 5, 2548−2558

Lewis acid sites on these catalysts (Figure S6 and Table 2). All the samples exhibit three main bands, that is, 1545 cm^{-1} corresponding to the band of pyridine protonated by Brønsted acid sites (pyridinium ions), 1455 cm^{-1} resulting from the band of pyridine coordinated to the Lewis acid sites (coordinatively unsaturated Al^{3+}), and 1490 cm^{-1} assigned to the pyridine associated with both Brønsted and Lewis sites.[15,45,46] No noticeable difference in the band intensity at 1545, 1490, and 1455 cm^{-1} can be found over these H-ZSM-5 samples with similar Si/Al ratios but different porous structures. On the other hand, the band intensity at 1455 cm^{-1} is much weaker than that at 1545 cm^{-1} and more than 90% of acid sites possess Brønsted acid nature (Table 2), which would severely impact the selectivity to acrolein in the glycerol dehydration.

3.3. Effect of Hierarchical Porous Structure on Glycerol Dehydration. As generally regarded in the previous literatures, the catalytic performance of the zeolites is greatly influenced by both acidity and porosity. The former determines the intrinsic activity and selectivity of the catalyst.,[5−7,9−15,17−22,26,29] while the latter contributes to improvement on the transportation of guest molecules, the accessibility to acid sites, and the tolerance capability for coke formation, which can further modify the performance of the catalysts.[18,31−35] As shown in the above results, the five catalysts possess almost the same Si/Al ratio (Table 1, XRF) and display minor difference in aluminum distribution (Figure 4c, Al maping). ^{27}Al MAS NMR spectra (Figure 5) and FT-IR spectra after pyridine adsorption (Figure S6 and Table 2) indicate that the aluminum atoms in all samples mainly exist in the tetrahedral framework sites with Brønsted acid nature, and NH_3-TPD plots (Figure S4 and Table 2) declare that these samples have similar amount and strength distribution of acid sites. Therefore, these five samples display comparable acidity in spite of their different mesopore topologies (Figures 1−4, S1, and S5 and Table 1), so that the relationship between the mesopore architecture and the catalytic performance can be clearly disclosed.

The catalytic dehydration of glycerol was conducted in the gaseous phase at 320 °C under the pressure of 1 bar, which is similar to the reaction conditions in literatures.[15,18,21,22] A glycerol aqueous solution with the concentration of 20 wt % was used as the feed and the WHSV of glycerol was fixed at 2.4 h^{-1}. No other carrier gas was used during the reaction. Figures 6 and 7 present the variations of the glycerol conversion and acrolein selectivity with the time-on-stream (TOS), respectively. The data at typical TOS are displayed in Table 3. It is found that all of the samples show the full conversion at the beginning of reaction, but they present significant differences in

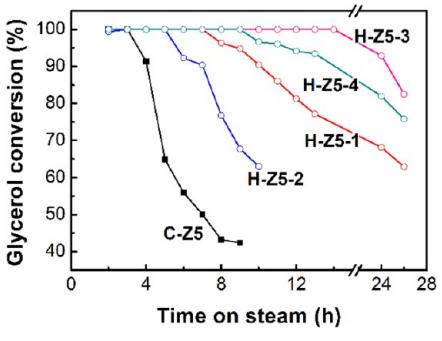

Figure 6. Glycerol conversion over different catalysts.

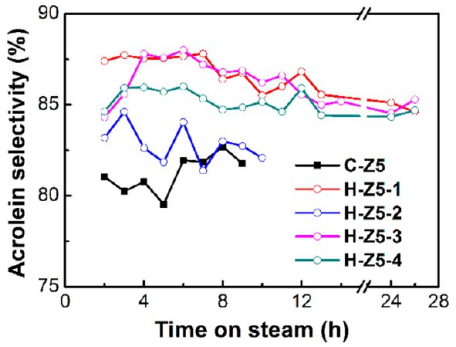

Figure 7. Acrolein selectivity over different catalysts.

the lifetime (Figure 6). The conventional C-Z5 catalyst undergoes the rapidest deactivation after 3 h. Its conversion even decreases to less than 45% after 8 h. Conversely, the four hierarchically structured catalysts all perform much slower deactivation than C-Z5. Their stabilities follow the order of H-Z5-3 > H-Z5-4 > H-Z5-1 > H-Z5-2. The H-Z5-3 with the highest stability can retain its high conversion over 92% for 24 h. Even in the worst case, H-Z5-2 also displays an improved catalytic performance compared with C-Z5. The turnover number (TON) is also calculated according to Figure 6 to evaluate their catalytic performance, which is defined as the moles of converted substrate on per mole of active centers before the deactivation of catalyst.[47,48] In this case, the mole of substrate is calculated based on mole of the converted glycerol, and the mole of active centers is obtained from the aluminum content in zeolite supposing that each aluminum atom in the framework corresponds to one acid site. In this paper, we define the TOS with 80% of glycerol conversion as the point for catalyst deactivation, and the TON values at 80% of conversion (TON_{80}) for C-Z5, H-Z5-1, H-Z5-2, H-Z5-3 and H-Z5-4 are 7.0×10^2, 1.9×10^3, 1.3×10^3, 4.7×10^3, and 3.9×10^3, respectively, as calculated by the eqs 1 and 2.

$$\mathrm{TON}_{80\%} = \frac{\text{mole of converted glycerol } (\geq 80\%)}{\text{mole of Al site in catalyst}} \times 100 \tag{1}$$

$$\text{mole of converted glycerol } (\geq 80\%) = \int_0^{t_{80\%}} \left(\frac{\text{WHSV value}}{\text{mole weight of glycerol}} \times \text{coversion} \right) dt \tag{2}$$

Besides the advantage of stability, the hierarchical zeolite catalysts also exhibit an improved acrolein selectivity compared to C-Z5, and their acrolein selectivity is almost unchanged with prolonging the reaction time even when the catalyst deactivation has begun (Figure 7). The average acrolein selectivity in 24 h follows the order of H-Z5-1 (86%) ≈ H-Z5-3 (86%) > H-Z5-4 (85%) > H-Z5-2 (83%). The main byproduct with the selectivity less than 12% is 1-hydroxyacetone resulting from the elimination of one water molecule from the terminal hydroxyl groups (Table 3), and other byproducts with the total selectivity below 7% include acetaldehyde, propanol, acetone, and traces of unidentified compounds. These high acrolein selectivities of the catalysts are closely related to the intrinsic acid nature of Brønsted acid sites (Figures 5 and S6 and Table 2) which could selectively interact with the secondary hydroxyl group in the comparatively small channels of zeolite, and eliminate two water molecules to result

DOI: 10.1021/cs5019953
ACS Catal. 2015, 5, 2548−2558

Table 3. Catalytic Performance for Glycerol Dehydration

				product selectivity (%)		
sample	WHSV (h^{-1})	TOS (h)	conversion (mol %)	acrolein	hydroxyacetone	others
C-Z5	2.4	2	100	81	8	11
		8	43	82	12	6
	12.0	2	73	86	9	5
		8	31	85	10	5
H-Z5-1	2.4	2	100	87	9	4
		10	90	86	10	4
	12.0	2	83	86	9	5
		8	45	87	9	4
H-Z5-2	2.4	2	100	83	10	7
		10	63	82	11	7
	12.0	2	81	86	8	6
		8	41	87	9	4
H-Z5-3	2.4	2	100	86	9	5
		10	100	86	11	3
	12.0	2	91	89	7	4
		8	74	88	8	4
H-Z5-4	2.4	2	100	85	9	6
		10	97	85	11	4
	12.0	2	88	89	7	4
		8	68	89	7	4

in a high acrolein selectivity.[6,7,16,18,20,21,28,29] The slight improved selectivity of acrolein (Figure 7) might be related to the effective withdrawing of the produced acrolein from the catalyst particles due to the high molecular transport rate of the mesopores, which greatly lowers the probability of the subsequent side reactions.[31,32]

The reactivity of these hierarchical zeolites was further evaluated either at a higher WHSV of 12 h^{-1} or at lower temperatures of 250, 280, and 300 °C. All other reaction conditions are kept the same as above and the results are shown in Table 3 and Figure 8. At a high WHSV of 12 h^{-1}, the

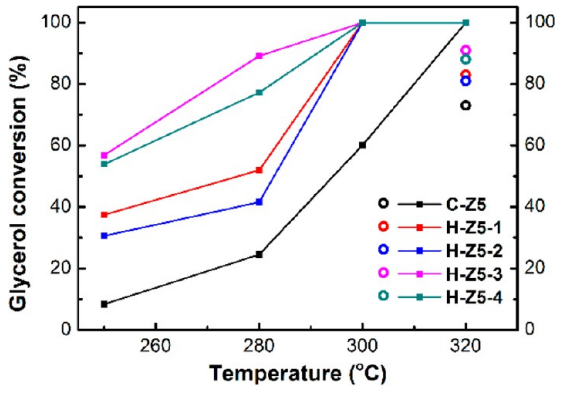

Figure 8. Glycerol conversion at different temperatures (line) or high WHSV of 12 h^{-1} (circle symbol) over different catalysts at initial reaction period of 2−3 h.

difference of the initial activities at TOS of 2 h could be well identified as H-Z5-3 (91%) > H-Z5-4 (88%) > H-Z5-1 (83%) > H-Z5-2 (81%) > C-Z5 (73%), while their selectivity and stability (cf. the conversion at 8 h, Table 3) present the similar order with the data at WHSV of 2.4 h^{-1} (Table 3). This tendency of activity can also be ascertained by lowering the reaction temperature. The glycerol conversion of all samples obviously decreases with the decrease of the reaction temperature (Figure 8), and their initial activities also follow the same order as those shown in Figure 6 and Table 3, i.e., H-Z5-3 > H-Z5-4 > H-Z5-1 > H-Z5-2 > C-Z5, at low temperature, especially in the cases of 250 and 280 °C.

The above catalytic reaction results have clearly proved the impacts of hierarchical porous structures on the improvement of activity, lifetime and selectivity on the glycerol dehydration (Table 3 and Figures 6−8). Although it has been generally believed that these positive effects result from the shorter transport path and enhanced coke tolerance in mesoporous zeolites,[18,31−35] the detailed relationships and working mechanisms are not so evidential. Therefore, in this paper, we are concerned about what type of hierarchical structure is more efficient and how these structures take effect on the glycerol dehydration via correlating the experiment results of mesoporous structure and those of reaction performance over our hierarchical samples with comparable microporisty and acidity but with different mesopore structures.

The relationships between the catalytic performance (lifetime and initial activity) and the structural properties ($V_{meso,N2}$, $V_{meso,Hg}$, and S_{meso}) are displayed in Figure 9. It clearly shows the positive roles of the mesopores on the improvement of the lifetime and activity despite of the existence of some complex factors. Figure 9a represents the relationship between the lifetime of these catalysts and their corresponding total mesopore volume measured by the adsorption of small-sized N_2 molecule ($V_{meso,N2}$). With the rise of $V_{meso,N2}$, the lifetime of these samples exhibits an interesting accelerated increase trend. And the special point of H-Z5-2 could be related to some special in-pore condensation of reactants or products, which will be explained below. Referring to the characterization results on their diverse mesopore architectures, that is, H-Z5-1 and H-Z5-2 possess the occluded mesopores with different size/amount, H-Z5-3 has enriched open and interconnected mesopores due to the nanocrystallite-assembly structure, and H-Z5-4 has both, several conclusions could be drawn, such as

DOI: 10.1021/cs5019953
ACS Catal. 2015, 5, 2548−2558

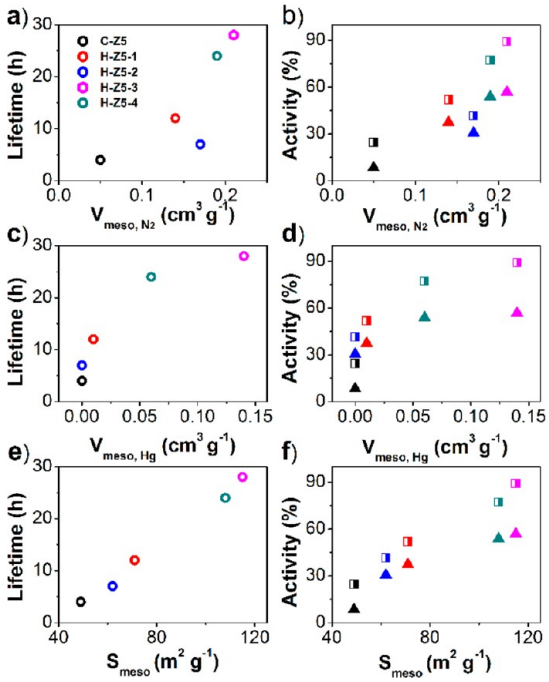

Figure 9. Plots of various structure-performance relationships for C-Z5 (black), H-Z5-1 (red), H-Z5-2 (blue), H-Z5-3 (magenta), and H-Z5-4 (cyan), where the mesoporisity parameters of $V_{meso,N2}$, $V_{meso,Hg}$, and S_{meso} are associated with the catalytic performance of lifetime on the left (circle, at 320 °C) and initial activity on the right (triangle, at 250 °C; cubic, at 280 °C). The catalyst lifetime is defined as the time for which the conversion exceeds the 80%, while the initial activity is defined as the glycerol conversion at initial reaction period of 2−3 h.

- the introduction of mesopores into zeolite catalysts is beneficial for extending the catalyst lifetime (comparing H-Z5-*x* with C-Z5);
- the open and interconnected mesopores (H-Z5-3 and H-Z5-4) take effect more efficiently than occluded intracrystal mesopores (H-Z5-1 and H-Z5-2);
- the relatively small-sized and occluded mesopores (H-Z5-2) might not be so suitable for glycerol dehydration.

On the other hand, the parameter of $V_{meso,Hg}$ provides an indicator of the accessible mesopore volume as detected by mercury intrusion from the crystal surface. Accordingly, the relationships between lifetime and $V_{meso,Hg}$ would fully rule out the effect of occluded mesopores. From Figure 9c, it can be clearly seen that the fast increase of the catalyst lifetime over $V_{meso,Hg}$ appears at the initial or near-zero stage ($V_{meso,Hg}$ = 0−0.01 cm^3/g) on H-Z5-1 and H-Z5-2, which further evidence that the sole presence of occluded mesopores in ZSM-5 zeolites can also promote the enhancement of catalyst lifetime in some extent.

As shown in Figure 9e, the catalyst lifetime seems strongly depend on the mesopore surface area of the zeolites. But the mesopore surface area derived by t-plot method is indeed a comprehensive parameter covering all the nonmicropore surface area including occluded mesopore surface area, open-mesopore surface area and the "real" crystal external surface. Generally, the resistance of hierarchical ZSM-5 zeolites to deactivation by coking is believed to correlate with the increased "external surface area"[49] (actually the surface area of nonmicropores, here denoted as S_{meso}). After comparatively analyzing the coked hierarchical samples, it is found that their capabilities to coke tolerance follow the order of H-Z5-3 > H-Z5-4 > H-Z5-1 ≈ H-Z5-2 (Figure 10, green bars) just in

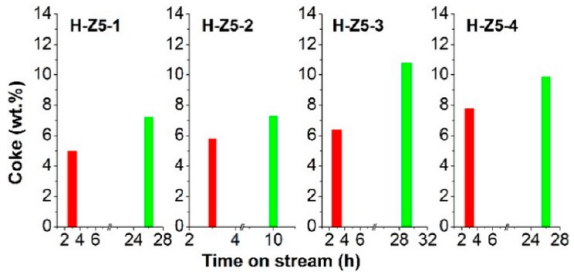

Figure 10. Coke formation for different hierarchical zeolites at the reaction of 3 h (red bars) and after reaction (green bars).

accordance with the trend of S_{meso}. This means that the existence of the mesopores is beneficial to the improvement of the capability for coke tolerance, especially in the case of the open mesopores (e.g., H-Z5-3). To further understand the role of mesoporosity on coke formation, the initial coking rates at TOS of 3 h were also measured (Figure 10, red bars). It is found that coke forms more rapidly in the initial stage, and then it would be slower until the catalyst deactivated (comparing green bars with red ones in Figure 10). Notably, the coking rates at the initial stage (red bars) do not match exactly with the capability for coke tolerance of the samples (green bars), especially the cases of H-Z5-2 > H-Z5-1 and H-Z5-4 > H-Z5-3 (red bars). Referring to the recent work of Hulteberg et al.,[27] the relative fast deactivation and low activity of H-Z5-2 may result from the physical condensation of glycerol or heavier derivatives in its small closed mesopore according to the Kelvin equation.[41] For the microporous zeolite, such as ZSM-5, the pore condensation or multimolecular reaction mechanism is sterically hindered in the micropores due to the similar pore size with the reactants.[22] However, the glycerol or heavier derivatives may condense in the mesopore and external surface regions. According to the Kelvin equation, the smaller the mesopore size the more serious the pore condensation.[27,41] Therefore, H-Z5-2 with abundant but smaller occluded mesopores more easily suffers the condensation of glycerol or heavier derivatives. Consistently, the pore condensation might also occurs in H-Z5-4 with small-sized occluded mesopores and then causes its relative lower activity and shorter lifetime than H-Z5-3. On the other hand, the results related to the initial activity of different catalysts (Figure 9b, d, and f) match well with that of catalyst lifetime (Figure 9a, c, and e), which reaffirm our previous conclusion.

In order to verify the improvement on the transport properties of these hierarchical ZSM-5 zeolites, their adsorption and diffusion properties are evaluated by studying the gravimetric uptake of *o*-xylene (its kinetic diameter is larger than the ZSM-5 pore size) on an IGA. The hierarchical ZSM-5 zeolites all exhibit higher adsorption isotherms than C-Z5 (Figure S7), indicating their higher adsorption capacity and rate. Their adsorption amount/rate follows the order of H-Z5-3 > H-Z5-4 > H-Z5-1 ≥ H-Z5-2 > C-Z5 over the range of test pressure, which matches well with the trend of their catalyst lifetime and activity.

3.4. Combined Effect of Acidity with Porous Structure on Glycerol Dehydration. The acidity is also a crucial parameter influencing the catalytic performance and stability for glycerol dehydration. Two hierarchical ZSM-5 catalysts with

DOI: 10.1021/cs5019953
ACS Catal. 2015, 5, 2548−2558

inter- and intracrystal mesopores but with low Si/Al ratio are employed to investigate the combined effect of acidity and porous structure. The first one (denoted as H-Z5-1-L) has the similar mesopore structure to H-Z5-1 (Figure 11a and b, ref

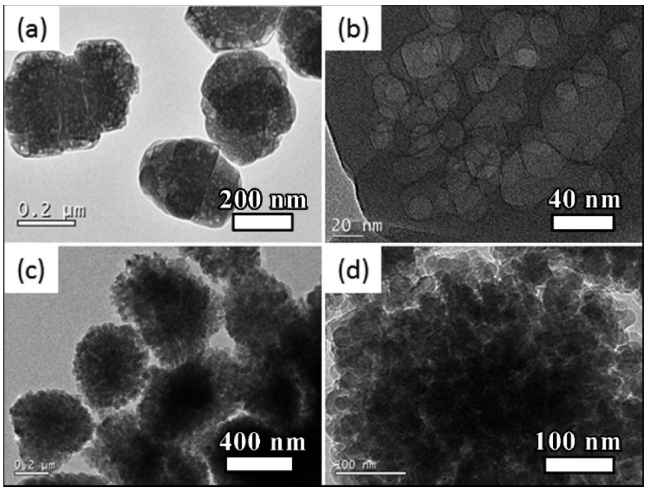

Figure 11. TEM images of (a and b) H-Z5-1-L and (c and d) H-Z5-3-L.

34), while the other (donated as H-Z5-3-L) is similar to H-Z5-3 (Figure 11c and d, ref 33). For the comparison, a conventional ZSM-5 zeolite with low Si/Al ratio (denoted as C-Z5-L) was adopted as a reference sample. The main features of these samples are listed in Table 4, and other characterization results were described elsewhere.[33,34] The XRF data in Table 4 show the similar Si/Al ratios of various samples. All samples have a large specific surface area and micropore volume. Comparably, the H-Z5-3-L of nanocrystallites oriented assembled structure possesses larger mesopore volume and mesopore surface area, while the H-Z5-1-L with abundant intracrystal mesopores possesses only larger mesopore volume with slightly increased mesopore surface area.

Table 4. Textural Properties and Chemical Composition of Different Zeolite Catalysts

sample	Si/Al[a]	S_L m^2/g	S_{meso}[b] m^2/g	V_{micro}[b] cm^3/g	$V_{meso,N2}$[c] cm^3/g
C-Z5-L	36	460	52	0.13	0.05
H-Z5-1-L	34	481	87	0.11	0.20
H-Z5-3-L	38	540	127	0.13	0.22

[a]Determined by XRF. [b]By *t*-plot method. [c]Using the BJH method. S_L: Langmuir surface area. S_{meso}: mesopore surface area.[38] V_{micro}: micropore volume. V_{meso}: mesopore volume.

For these ZSM-5 catalysts with low Si/Al ratio, their product distributions are similar to those with high Si/Al ratio, where acrolein (ca. 84%) is also the main product. The glycerol conversion and selectivity for acrolein over TOS are shown in Figure 12. The hierarchical samples with low Si/Al ratio, both for H-Z5-3-L and H-Z5-1-L, only show small improvement for catalyst deactivation compared with the conventional ZSM-5 catalyst (C-Z5-L). For example, the glycerol conversions after 8 h are 53, 72, and 74% for C-Z5-L, H-Z5-1-L, and H-Z5-3-L, respectively. Whereas the acrolein selectivity is similar for these two hierarchical ones (85 and 84%), but slight higher than that of C-Z5-L (82%).

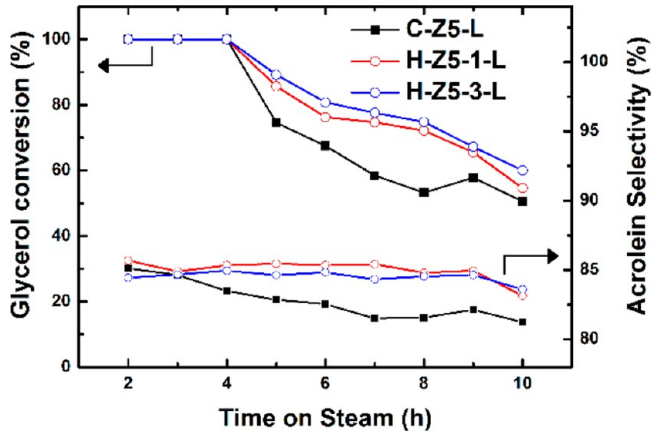

Figure 12. Glycerol conversion and acrolein selectivity over different catalysts at reaction temperature of 320 °C and WHSV of 2.4 h^{-1}.

Combining with previous results on conventional microporous zeolite, the catalytic performance of C-Z5 is worse than that of C-Z5-L not only on the glycerol conversion but also on the acrolein selectivity. These results are consistent with literature results for zeolite catalysts.[20−22] In view of the difficult internal diffusion and few external surface acid sites of conventional zeolites, the high amount/density of acid sites on the low Si/Al samples may lead to a better glycerol conversion and acrolein selectivity.[20−22] However, for hierarchical structured ZSM-5 catalysts, the cases are different. Only those with high Si/Al ratio present notable activity, selectivity, and long-term stability, while the one with low Si/Al ratio (H-Z5-1-L and H-Z5-3-L) display slight improvements over the conventional sample (C-Z5-L). The reaction results demonstrate that the combined effect of acidity and porous structure should be considered for glycerol dehydration. Considering the enhanced accessibility to acid sites and improved molecular transport of reactant/product in the microporous crystals, the hierarchical catalysts of high Si/Al ratio may be more suitable for the glycerol dehydration. The excessive amount/density of acid sites in H-Z5-1-L and H-Z5-3-L would tend to promote the multimolecular reactions or side reactions which will generate the byproducts and rapid deactivation through the complex reaction network, including a series of polycondensation reactions and other secondary reactions such as oligomerization, cyclization, aromatization, and hydrogen transfer reactions.[7,15,19,20,22]

4. CONCLUSION

Four typical hierarchical ZSM-5 zeolites with a series of mesopore architectures, covering the mesopore size, distribution, and connectivity, have been successfully prepared through our previously developed approach of "salt-aided seed-induced route". In view of these mesoporous zeolites with comparable microporosity and acidity, the effect of hierarchical architecture could be systematically investigated for the reaction of glycerol dehydration. The catalytic results demonstrate that these hierarchically structured zeolites indeed exhibit strongly enhanced catalytic activity, stability, and selectivity compared with the conventional ZSM-5 zeolite, and the open and interconnected mesopore architectures (H-Z5-3 and H-Z5-4) are more effective than closed ones (H-Z5-1 and H-Z5-2). Interestingly, the existence of small intracrystal mesopore might lead to a shorter lifetime and worse activity (H-Z5-2 < H-Z5-1,

DOI: 10.1021/cs5019953
ACS Catal. 2015, 5, 2548−2558

H-Z5-4 < H-Z5-3). This abnormal catalytic performance can be well-explained by the proposal of pore condensation of glycerol or its heavier derivatives. Finally, through tuning the Si/Al ratio, the interplay between the catalytic performance and acidity indicates the necessity of the combination of hierarchical structure and suitable acidity on this reaction. This work will guide us to construct the efficient zeolite catalysts in term of pore structure engineering and acidity modification for the dehydration of glycerol to acrolein.

■ ASSOCIATED CONTENT

Supporting Information

The following file is available free of charge on the ACS Publications website at DOI: 10.1021/cs5019953.

Some detailed information on these catalysts, including Ar adsorption characterization, O mapping images, XRD patterns, NH_3-TPD profiles, potentiometric titration curves with *tert*-butylamine, FT-IR spectra after pyridine adsorption, and *o*-xylene adsorption measurement (PDF)

■ AUTHOR INFORMATION

Corresponding Authors

*E-mail: yitang@fudan.edu.cn (Y.T.).
*E-mail: shuhl@fudan.edu.cn (H.X.).

Notes

The authors declare no competing financial interest.

■ ACKNOWLEDGMENTS

This work was supported by National Key Basic Research Program of China (2013CB934101), STCSM (11JC1400400 and 14120700700), and National Plan for Science and Technology (14-PET827-02).

■ REFERENCES

(1) Huber, G. W.; Iborra, S.; Corma, A. *Chem. Rev.* **2006**, *106*, 4044−4098.
(2) Ragauskas, A. J.; Williams, C. K.; Davison, B. H.; Britovsek, G.; Cairney, J.; Eckert, C. A.; Frederick, W. J.; Hallett, J. P.; Leak, D. J.; Liotta, C. L.; Mielenz, J. R.; Murphy, R.; Templer, R.; Tschaplinski, T. *Science* **2006**, *311*, 484−489.
(3) Corma, A.; Iborra, S.; Velty, A. *Chem. Rev.* **2007**, *107*, 2411−2502.
(4) ten Dam, J.; Hanefeld, U. *ChemSusChem* **2011**, *4*, 1017−1034.
(5) Katryniok, B.; Paul, S.; Belliere-Baca, V.; Rey, P.; Dumeignil, F. *Green Chem.* **2010**, *12*, 2079−2098.
(6) Katryniok, B.; Paul, S.; Capron, M.; Dumeignil, F. *ChemSusChem* **2009**, *2*, 719−730.
(7) Katryniok, B.; Paul, S.; Dumeignil, F. *ACS Catal.* **2013**, *3*, 1819−1834.
(8) Pagliaro, M.; Ciriminna, R.; Kimura, H.; Rossi, M.; Della Pina, C. *Angew. Chem., Int. Ed.* **2007**, *46*, 4434−4440.
(9) Atia, H.; Armbruster, U.; Martin, A. *J. Catal.* **2008**, *258*, 71−82.
(10) Chai, S. H.; Wang, H. P.; Liang, Y.; Xu, B. Q. *Green Chem.* **2008**, *10*, 1087−1093.
(11) Tsukuda, E.; Sato, S.; Takahashi, R.; Sodesawa, T. *Catal. Commun.* **2007**, *8*, 1349−1353.
(12) Chai, S. H.; Wang, H. P.; Liang, Y.; Xu, B. Q. *J. Catal.* **2007**, *250*, 342−349.
(13) Chai, S. H.; Wang, H. P.; Liang, Y.; Xu, B. Q. *Green Chem.* **2007**, *9*, 1130−1136.
(14) Ulgen, A.; Hoelderich, W. G. *Catal. Lett.* **2009**, *131*, 122−128.
(15) Kim, Y. T.; Jung, K. D.; Park, E. D. *Microporous Mesoporous Mater.* **2010**, *131*, 28−36.
(16) Kongpatpanich, K.; Nanok, T.; Boekfa, B.; Probst, M.; Limtrakul, J. *Phys. Chem. Chem. Phys.* **2011**, *13*, 6462−6470.
(17) Yoda, E.; Ootawa, A. *Appl. Catal., A* **2009**, *360*, 66−70.
(18) Jia, C. J.; Liu, Y.; Schmidt, W.; Lu, A. H.; Schuth, F. *J. Catal.* **2010**, *269*, 71−79.
(19) Possato, L. G.; Diniz, R. N.; Garetto, T.; Pulcinelli, S. H.; Santilli, C. V.; Martins, L. *J. Catal.* **2013**, *300*, 102−112.
(20) de Oliveira, A. S.; Vasconcelos, S. J. S.; de Sousa, J. R.; de Sousa, F. F.; Filho, J. M.; Oliveira, A. C. *Chem. Eng. J.* **2011**, *168*, 765−774.
(21) Carrico, C. S.; Cruz, F. T.; Santos, M. B.; Pastore, H. O.; Andrade, H. M. C.; Mascarenhas, A. J. S. *Microporous Mesoporous Mater.* **2013**, *181*, 74−82.
(22) Kim, Y. T.; Jung, K. D.; Park, E. D. *Appl. Catal., A* **2011**, *393*, 275−287.
(23) Corma, A. *Chem. Rev.* **1997**, *97*, 2373−2419.
(24) Kubicka, D.; Kubickova, I.; Cejka, J. *Catal. Rev.: Sci. Eng.* **2013**, *55*, 1−78.
(25) Corma, A.; Huber, G. W.; Sauvanauda, L.; O'Connor, P. *J. Catal.* **2008**, *257*, 163−171.
(26) Suprun, W.; Lutecki, M.; Haber, T.; Papp, H. *J. Mol. Catal. A: Chem.* **2009**, *309*, 71−78.
(27) Hulteberg, C.; Leveau, A.; Brandin, J. G. M. *Top. Catal.* **2013**, *56*, 813−821.
(28) Kinage, A. K.; Upare, P. P.; Kasinathan, P.; Hwang, Y. K.; Chang, J. S. *Catal. Commun.* **2010**, *11*, 620−623.
(29) Alhanash, A.; Kozhevnikova, E. F.; Kozhevnikov, I. V. *Appl. Catal., A* **2010**, *378*, 11−18.
(30) Chal, R.; Gerardin, C.; Bulut, M.; van Donk, S. *ChemCatChem* **2011**, *3*, 67−81.
(31) Chen, L. H.; Li, X. Y.; Rooke, J. C.; Zhang, Y. H.; Yang, X. Y.; Tang, Y.; Xiao, F. S.; Su, B. L. *J. Mater. Chem.* **2012**, *22*, 17381−17403.
(32) Perez-Ramirez, J.; Christensen, C. H.; Egeblad, K.; Christensen, C. H.; Groen, J. C. *Chem. Soc. Rev.* **2008**, *37*, 2530−2542.
(33) Zhang, H. B.; Ma, Y. C.; Song, K. S.; Zhang, Y. H.; Tang, Y. *J. Catal.* **2013**, *302*, 115−125.
(34) Zhang, H. B.; Song, K. S.; Wang, L.; Zhang, H. X.; Zhang, Y. H.; Tang, Y. *ChemCatChem* **2013**, *5*, 2874−2878.
(35) Perez-Ramirez, J.; Abello, S.; Bonilla, A.; Groen, J. C. *Adv. Funct. Mater.* **2009**, *19*, 164−172.
(36) Bonilla, A.; Baudouin, D.; Perez-Ramirez, J. *J. Catal.* **2009**, *265*, 170−180.
(37) Hu, Z.; Zhang, H.; Wang, L.; Zhang, H.; Zhang, Y.; Xu, H.; Shen, W.; Tang, Y. *Catal. Sci. Technol.* **2014**, *4*, 2891−2895.
(38) Milina, M.; Mitchell, S.; Crivelli, P.; Cooke, D.; Perez-Ramirez, J. *Nat. Commun.* **2014**, *5*, 3922.
(39) Mitchell, S.; Michels, N. L.; Kunze, K.; Perez-Ramirez, J. *Nat. Chem.* **2012**, *4*, 825−831.
(40) Znaiguia, R.; Brandhorst, L.; Christin, N.; Baca, V. B.; Rey, P.; Millet, J. M. M.; Loridant, S. *Microporous Mesoporous Mater.* **2014**, *196*, 97−103.
(41) Monson, P. A. *Langmuir* **2008**, *24*, 12295−12302.
(42) Zhan, B. Z.; White, M. A.; Lumsden, M.; Mueller-Neuhaus, J.; Robertson, K. N.; Cameron, T. S.; Gharghouri, M. *Chem. Mater.* **2002**, *14*, 3636−3642.
(43) Groen, J. C.; Peffer, L. A. A.; Pérez-Ramírez, J. *Microporous Mesoporous Mater.* **2003**, *60*, 1−17.
(44) Thommes, M. *Chem. Ing. Technol.* **2010**, *82*, 1059−1073.
(45) Chakraborty, B.; Viswanathan, B. *Catal. Today* **1999**, *49*, 253−260.
(46) Buzzoni, R.; Bordiga, S.; Ricchiardi, G.; Lamberti, C.; Zecchina, A.; Bellussi, G. *Langmuir* **1996**, *12*, 930−940.
(47) Kozuch, S.; Martin, J. M. L. *ACS Catal.* **2012**, *2*, 2787−2794.
(48) Umpierre, A. P.; de Jesus, E.; Dupont, J. *ChemCatChem* **2011**, *3*, 1413−1418.
(49) Kim, J.; Choi, M.; Ryoo, R. *J. Catal.* **2010**, *269*, 219−228.

DOI: 10.1021/cs5019953
ACS Catal. 2015, 5, 2548−2558